A theoretical assessment of excited states gradients and resonance Raman intensities for the azobenzene molecule

Magdalena Staniszewska[a], Stephan Kupfer[b], Marta Łabuda[a], Julien Guthmuller[a]*

[a] Faculty of Applied Physics and Mathematics, Gdańsk University of Technology, Narutowicza 11/12, 80-233 Gdańsk, Poland

[b] Institute of Physical Chemistry, Friedrich Schiller University Jena, Helmholtzweg 4, 07-743 Jena, Germany

Abstract

The ground state geometries and vibrational frequencies as well as the excitation energies and excited state gradients of the $S_1(n\pi^*)$ and $S_2(\pi\pi^*)$ states of *trans-* and *cis*-azobenzene are investigated by several DFT methods, namely B3LYP, PBE, M06-2X, CAM-B3LYP and ωB97X. Excited state properties and in particular gradients are also assessed using the wave function based methods EOM-CCSD and RASPT2/RASSCF. Comparison with experimental data shows that the B3LYP functional gives the most accurate results for the ground state geometry and vibrational frequencies. The analysis of the vertical excitation energies reveals that the RASPT2 approach provides the most accurate excitation energies with deviations of the order of 0.1 eV. Among the TDDFT methods, the CAM-B3LYP functional shows the best performance on the excitation energies. By assessing the excited state gradients with respect to the reference RASPT2 data, the most accurate gradients are obtained with B3LYP, whereas other functionals as well as the EOM-CCSD and RASSCF calculations give less consistent results. Overall, despite the tendency of B3LYP to underestimate the excitation energies, this functional provides the most balanced description of both ground and excited state properties for both isomers of azobenzene in the Franck-Condon region.

1. Introduction

The calculation of molecular properties for small and medium sized organic compounds in the electronic ground state can be considered nowadays almost routine. In this case, the most widely applied method is density functional theory (DFT). In particular, it has been shown that hybrid functionals can give an accurate description of equilibrium geometries, dipole moments and vibrational frequencies, see e.g., refs[1,2]. However, the calculation of excited state properties is more challenging for quantum chemistry and many methods were proposed. Among them, the most popular approach is time-dependent DFT[3,4,5] (TDDFT), due to its good compromise between accuracy and computational cost. Nevertheless, several wave function based methods are also widely in use and aim at providing higher accuracy than TDDFT at the prize of a reasonably increased computational cost. In particular, multiconfigurational methods, such as the RASPT2[6]/RASSCF[7,8] (Restricted Active Space Perturbation Theory of second order/Restricted Active Space Self-Consistent Field) or the well-established CASPT2[9]/CASSCF[10] (Complete Active Space Perturbation Theory of second order/Complete Active Space SCF) approaches are able to deliver a reliable description of excited states, irrespective of the wave functions character. Moreover, different methods derived from the Coupled Cluster (CC) theory are available and have shown good accuracies in the determination of excited states energies,[11,12] as e.g. the equation of motion coupled cluster method restricted to single and double excitations[13] (EOM-CCSD). One can also mention the recent use of the density matrix renormalization group (DMRG) method,[14,15] which present great potentialities for the calculation of systems requiring a large number of active orbitals.[16,17]

To identify the advantages and disadvantages of these methods, a number of studies have evaluated the calculated excited states properties, by comparing them either with experimental results or with reference theoretical data. This has mainly concerned the calculation of singlet and triplet vertical excitation energies as well as transition dipole moments, see e.g., refs[18,19,20,21,22]. However, less is known about the accuracy of quantum chemistry methods for the determination of excited state

gradients, which are important for a correct evaluation of excited state geometries and for the treatment of excited state dynamics. Therefore, a better knowledge of the performance of standard computational approaches is very desirable. The calculation of excited state geometries and Franck-Condon (FC) factors allows the simulation of the vibronic structure in absorption or electronic circular dichroism spectra. Such effects were investigated in previous studies (see e.g. refs[23,24,25,26,27]), and benchmarking of the theoretical methods was made by comparison with experimental results. However, such a comparison hardly allows to estimate the calculated geometrical displacements or gradients along the individual coordinates, due to the usually limited resolution of the vibronic structure in the experimental spectra. Therefore, several studies[28,29,30] made use of resonance Raman (RR) spectroscopy simulations[31,32,33,34,35,36,37,38] to assess the excited state gradients along each vibrational coordinate. Indeed, within the so-called short-time or gradient approximation,[39] the RR intensities are directly related to the excited state gradients evaluated at the electronic ground state geometry. In this respect, the calculation of RR intensities and their comparison with experimental data provides an opportunity for assessing the ability of quantum chemistry methods to determine excited state gradients.
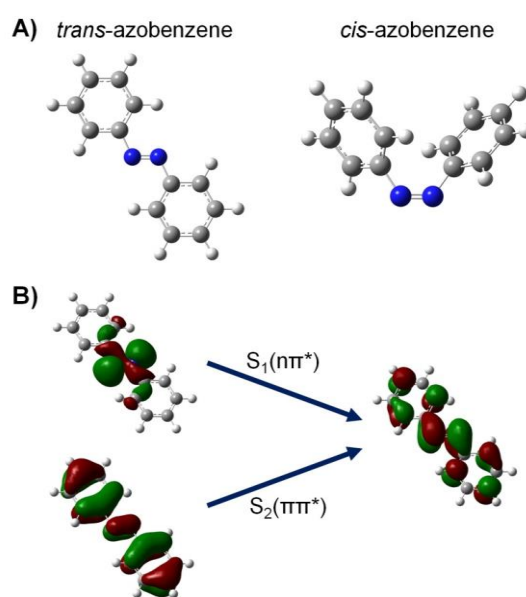

Figure 1: A) Structures of the azobenzene isomers. B) Main DFT frontier orbitals involved in the two first singlet excited states of *trans*-azobenzene.

This study investigates the gradients and RR spectra of the well-known molecule of azobenzene for both isomers i.e. *trans*-azobenzene and *cis*-azobenzene (Figure 1A). Azobenzene has attracted much interest due to its reversible *trans→cis* isomerization of the N=N bond upon photoexcitation. Hence, based on this photo-switchable property, a wide range of applications[40,41] have been proposed for azobenzene e.g. in information storage, as molecular motors or as photoswitch in biological systems. However, the detailed pathways underlying the isomerization are still a matter of extensive debate among experimentalists[42,43,44,45,46,47,48,49,50,51] and theoreticians.[52,53,54,55,56,57,58,59,60,61,62,63,64,65] The elucidation of the photoisomerization dynamics requires a precise characterization of the potential energy surfaces (PESs) of the two first excited states, namely the weakly-absorbing n→π* (S_1) and the strongly-absorbing π→π* (S_2) transitions (Figure 1B). In particular, several computational studies[66,67,68,52,54,55,56,59,62] have investigated the dynamics of azobenzene and of some derivatives on the S_1(nπ*) and S_2(ππ*) PESs. The predictions obtained by these works rely on the accuracy of the calculated PESs properties, which are usually determined by quantum chemistry methods. Therefore, an assessment of commonly employed methods is highly desirable for azobenzene, in order to evaluate their ability to describe excited state properties i.e. transition energies and gradients. The excitation energies of azobenzene and its several derivatives were investigated by TDDFT and it was concluded that hybrid functionals, like PBE0[69] or B3LYP,[70,71] provide a good reproduction of the ground state properties, whereas long-range corrected functionals, like CAM-B3LYP,[72] give accurate values for transition energies.[73,74] Multiconfigurational and CC calculations of excited state energies were also reported in several studies (see e.g. refs[58,60,63,75,76,65]). However, a systematic assessment of excited state gradients was not yet reported for azobenzene, despite the importance of these quantities for the simulation of its excited state dynamics. Moreover, no detailed theoretical study of the azobenzene RR spectra is available in the literature, whereas experimental investigations were performed and have provided valuable information concerning the elucidation of the isomerization mechanism.[46,77,44] Therefore, in this work TDDFT, EOM-CCSD and RASPT2/RASSCF approaches are applied for the

computation of the $S_1(n\pi^*)$ and $S_2(\pi\pi^*)$ excited state properties of both isomers. The obtained results are compared with experimental data recorded via RR spectroscopy.[46] This comparison provides information about the excited states gradients calculated at the ground state geometry (i.e. FC point) and for totally symmetric normal modes, for which the gradients are non-vanishing.

The present article is organized as follows: Section 2 presents the computational methods employed to calculate the gradients and the RR intensities. In section 3, the geometries (3.1), excitation energies (3.2) and excited state gradients (3.3 and 3.4) are assessed with respect to experimental results. In section 3.5, the obtained gradients are compared with reference theoretical data. Finally, section 4 contains some conclusive remarks.

2. Computational methods

Calculations were carried out for both isomers of azobenzene without applying symmetry constraint. DFT and second-order Møller-Plesset (MP2) methods were employed to calculate the geometry, harmonic vibrational frequencies and normal coordinates in the ground state. The DFT calculations were performed with the B3LYP,[70,71] PBE,[78] M06-2X,[79] CAM-B3LYP[72] and ωB97X[80] exchange-correlation (XC) functionals in association with the 6-311++G(d,p) basis set. The MP2 calculations made use of the 6-311G(d,p) basis set. To correct for the lack of anharmonicity and the approximate treatment of electron correlation,[81] the harmonic frequencies obtained with B3LYP, PBE, M06-2X, CAM-B3LYP, ωB97X and MP2 were scaled by factors of 0.98, 1.00, 0.95, 0.95, 0.95 and 0.98, respectively. Additionally, the effects of the solvent ethanol ($\varepsilon = 24.852$) on the ground state properties were taken into account by the integral equation formalism of the polarizable continuum model[82] (IEFPCM). Calculations in a vacuum were also performed with the B3LYP functional.

The vertical excitation energies, oscillator strengths and analytical Cartesian energy derivatives (gradients) of the $S_1(n\pi^*)$ and $S_2(\pi\pi^*)$ excited states were obtained from TDDFT calculations employing the 6-311++G(d,p) basis set. The TDDFT calculations were performed by using the same XC functionals as for the ground state properties. Moreover, the excited state properties were also determined with all previously mentioned XC functionals by employing the B3LYP ground state geometry, frequencies and normal coordinates calculated in ethanol. These calculations are referred to as TD-ESM//GSM, in which ESM indicates the method employed for the excited state properties and GSM indicates the method employed for the ground state properties. The excited state properties were calculated in a vacuum and in ethanol. In the latter case, the effects of the solvent were approximated with IEFPCM and the non-equilibrium procedure of solvation was used for the computation of the excitation energies and excited state gradients.

The excitation energies, oscillator strengths and gradients of the $S_1(n\pi^*)$ and $S_2(\pi\pi^*)$ excited states were also evaluated with EOM-CCSD. The EOM-CCSD calculations were performed in a vacuum

using the B3LYP ground state geometry in ethanol. The 6-311++G(d,p) basis set was employed for the excitation energies and the 6-31G(d) basis set was used to calculate the gradients.

All computations described previously were carried out by means of the Gaussian 09 program.[83] The EOM-CCSD excited state gradients were obtained by a two-point numerical differentiation procedure from the vertical excitation energies, which were computed for distorted structures resulting from the addition or subtraction of a finite displacement along the normal coordinates to the ground state geometry. These gradients were calculated with a program developed locally.[28,38]

The excitation energies, oscillator strengths and gradients of the $n\pi^*$ and $\pi\pi^*$ excited states of interest were also investigated by state-of-the-art multiconfigurational methods, namely with the RASSCF and RASPT2 approaches. The RASSCF and RASPT2 calculations were performed in a vacuum using the B3LYP ground state geometry optimized in ethanol. The large 6-311++G(d,p) basis set was also employed in this case and the RASPT2/RASSCF calculations were realized with the Molcas 8.0 program.[84] The Cholesky decomposition[85] was applied to generate the two-electron integrals. In order to specify the restricted active spaces (RASs) used in the calculations, the notation RAS($n,l,m;i,j,k$) of Gagliardi and co-workers[19] was adopted. The index n labels the number of active electrons, l is the maximum number of holes in the RAS1, and m is the maximum number of electrons in the RAS3. The labels i, j and k refer to the number of active orbitals in the RAS1, RAS2, and RAS3, respectively. Two different RAS partitions were considered, namely RAS(18,2,2;7,3,6) and RAS(18,4,4;9,0,7), where both partitions comprise all seven pairs of $\pi\pi^*$ orbitals as well as the two non-bonding p-orbitals of the nitrogen atoms. The RAS(18,2,2;7,3,6) includes in the RAS2 the three molecular orbitals involved in the leading transitions of the $S_1(n\pi^*)$ and $S_2(\pi\pi^*)$ states obtained at the TDDFT level of theory, that is, one non-bonding nitrogen-centered orbital (n_2), one bonding π-orbital (π_7) and one antibonding π-orbital (π_7^*). The remaining six bonding orbitals (π_1-π_6) as well as the second non-bonding nitrogen-centered orbital (n_1) and the six antibonding orbitals (π_1^*-π_6^*) were assigned to the RAS1 and RAS3 partitions, respectively. An interaction among the subspaces of up to double excitations was taken into account, spanning over

12601 configuration state functions (CSFs). The RAS(18,4,4;9,0,7) features the same molecular orbitals as described previously for the RAS(18,2,2;7,3,6). However, all occupied and virtual orbitals were distributed along the RAS1 and RAS3, respectively, according to the Hartree-Fock (HF) wave function. Excitations among the RAS1 and RAS3 were considered up to the quadruple level. This computational setup leads in consequence to a number of 274450 CSFs. Both RASs are illustrated exemplarily for the *trans*-isomer in Figure 2, while the RASs for the *cis*-isomer are shown in Figure S1 of the supporting information.
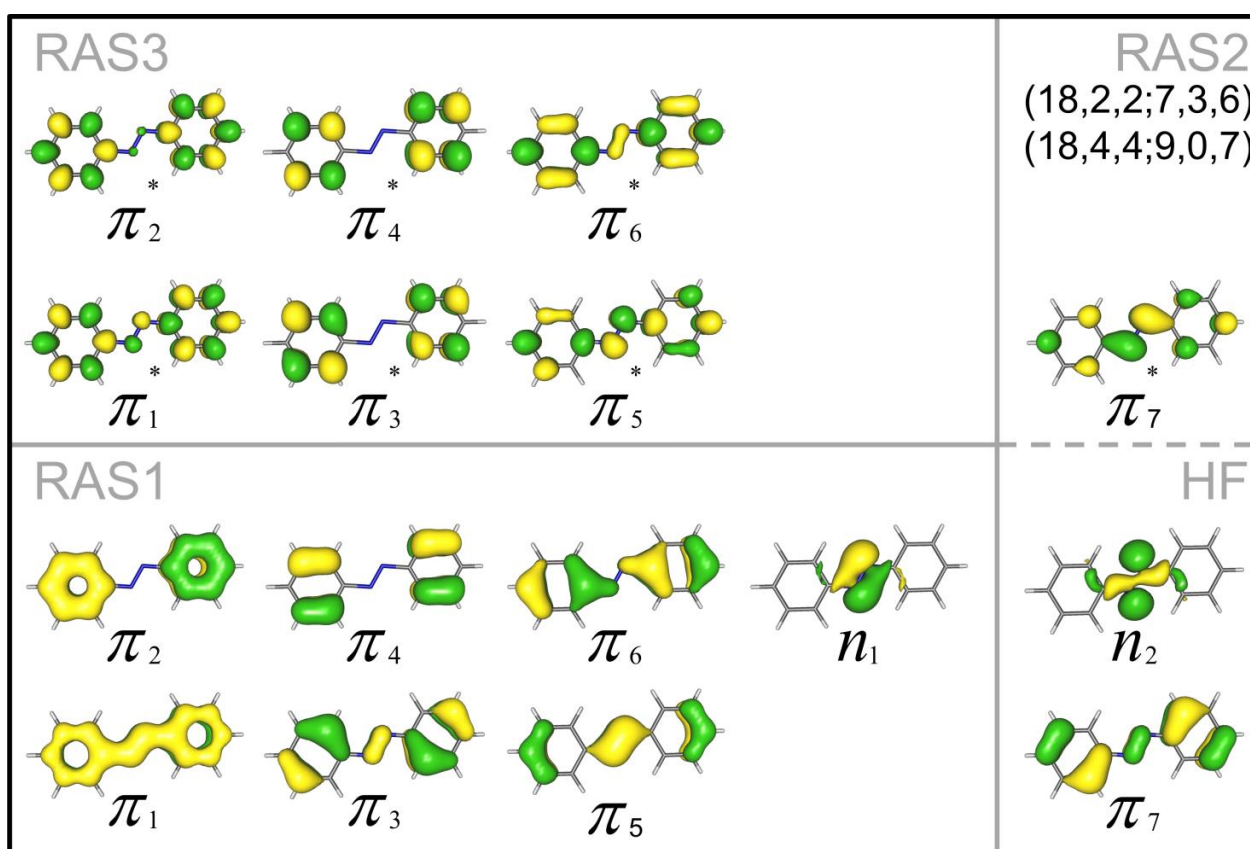

Figure 2: Illustration of RAS(18,2,2;7,3,6) and RAS(18,4,4;9,0,7) employed in the multiconfigurational RASPT2/RASSCF calculations of *trans*-azobenzene. The occupation of the Hartree-Fock ground state wave function is indicated by a dashed grey line.

State-average (SA-) RASSCF calculations were performed for both RAS partitions, while the first six and the first eight roots have been considered for RAS(18,2,2;7,3,6) and RAS(18,4,4;9,0,7), respectively. Subsequently, dynamical correlation was included by means of multi-state (MS-)

RASPT2, while the core electrons were treated as frozen and a level shift of 0.3 a.u. was applied. The oscillator strengths have been obtained at the SA-RASSCF and MS-RASPT2 levels of theory with the CAS State Interaction method.[86] The numerical gradients have been calculated for the $n\pi^*$ and the $\pi\pi^*$ states of both isomers (*cis* and *trans*) at the SA-RASSCF and the MS-RASPT2 levels of theory.

The relative resonance Raman (RR) intensities for an excitation in resonance with the $S_1(n\pi^*)$ or $S_2(\pi\pi^*)$ excited states were obtained within the short-time approximation[39] (STA), also known as the gradient method. In the STA, the relative RR intensities for fundamental transitions $0 \rightarrow 1_n$ are obtained from the gradients i.e. from the partial derivatives of the excited state electronic energy (E^e) along the nth normal coordinates (Q_n) evaluated at the ground state equilibrium geometry:

$$I_{0 \rightarrow 1_n} \propto \frac{1}{\omega_n} \left(\frac{\partial E^e}{\partial Q_n} \right)_0^2 \tag{1}$$

where ω_n is the frequency of the nth normal mode.

3. Results

3.1. Ground state geometries.

The ground state geometries of *trans*- and *cis*-azobenzene were optimized by MP2 as well as by DFT using the B3LYP, PBE, M06-2X, CAM-B3LYP and ωB97X XC functionals. These geometries were calculated in ethanol using a PCM. The choice of the solvent is motivated by available experimental RR spectra[46] to which our calculations will be compared to (see section 3.3.). Additionally, the geometries were also computed in a vacuum with the B3LYP XC functional. The root mean square (RMS) deviations between the calculated and experimental geometries are reported in Table 1, whereas details of the bond lengths and bond angles can be found in the supporting information (Figure S2 and Tables S1-S5). The theoretical geometries are compared to experimental X-ray data obtained in the solid state[87,88,89] and to electron diffraction data measured in gas phase.[90] The results obtained with B3LYP indicate that the solvent has small effects on the geometries, and that both structures calculated in a vacuum or in ethanol compare equivalently well to the experimental data. The geometries calculated with MP2 or with the other XC functionals present a comparable accuracy as the B3LYP results. In the case of *trans*-azobenzene, the RMS deviations are in most cases below 0.01 Å for the bond lengths and below 1° for the bond angles, whereas deviations for *cis*-azobenzene are slightly larger. Based on this comparison, it can be concluded that all employed methods provide geometries in good agreement with the experimental data. However, comparison with only the electron diffraction data measured in gas phase indicates that the B3LYP and PBE XC functionals as well as MP2 are the most accurate. The *trans*-azobenzene structure is planar in all cases, whereas *cis*-azobenzene is found with C-N-N-C dihedral angles of 9.4, 11.5, 7.1, 7.3, 6.0 and 6.8°, as well as with C-C-N-N dihedral angles of 51.6, 48.8, 54.3, 55.6, 57.7 and 55.6° for B3LYP, PBE, M06-2X, CAM-B3LYP, ωB97X and MP2, respectively. These values are in good agreement with the experimental X-ray values[89] of 8.0 and 53.3° for the C-N-N-C and C-C-N-N dihedral angles, respectively.

Table 1: Comparison between experimental and calculated ground state geometries of *trans-* and *cis*-azobenzene. The RMS deviations are given for bond lengths and bond angles.

Methods	Bond length RMS deviations (Å)			Bond angles RMS deviations (°)	
	trans-azobenzene		*cis*-azobenzene	*trans*-azobenzene	*cis*-azobenzene
	X-ray[a]	ED[b]	X-ray[a]	X-ray[a]	X-ray[a]
B3LYP[c]	0.010	0.007	0.012	0.66	1.05
B3LYP[d]	0.010	0.007	0.014	0.74	1.04
PBE[d]	0.017	0.007	0.017	0.68	1.00
M06-2X[d]	0.007	0.009	0.014	0.48	0.86
CAM-B3LYP[d]	0.005	0.010	0.013	0.63	0.89
ωB97X[d]	0.006	0.009	0.014	0.50	0.85
MP2[d]	0.016	0.005	0.017	0.53	0.97

[a] The experimental X-ray data in the solid state are taken from references.[88,89] [b] The experimental electron diffraction (ED) data in gas phase are taken from reference.[90] [c] Geometry calculated in a vacuum. [d] Geometry calculated in ethanol using PCM.

3.2. Excited states excitation energies.

The excitation energies of the $S_1(n\pi^*)$ and $S_2(\pi\pi^*)$ excited states were first calculated using the TDDFT method. The results for both isomers are reported in Table 2 and are compared to experimental data. Additional details about the excited states including orbital characters, transition weights and oscillator strengths can be found in the supporting information (Tables S6-S9). The calculations were performed in ethanol with all considered XC functionals, whereas calculations in a vacuum were also realized with B3LYP. Comparing these latter results with experimental data obtained in gas phase shows that B3LYP underestimates the excitation energies by 0.27 and 0.43 eV for the $S_1(n\pi^*)$ and the $S_2(\pi\pi^*)$ states of *trans*-azobenzene, respectively, and by 0.36 eV and 0.59 eV for the $S_1(n\pi^*)$ and $S_2(\pi\pi^*)$ states of *cis*-azobenzene, respectively. Note that the experimental value (4.68 eV) for the $S_2(\pi\pi^*)$ state of *cis*-azobenzene is taken from Andersson et al.[91] and is associated to a shoulder in the measured gas phase spectrum. This shoulder is assigned to a $\pi\pi^*$ transition and might originate from the contribution of several excited states. For example, based on CC2 calculations it was assigned to the $S_4(\pi\pi^*)$ state by Fliegl et al.[76]. Therefore, it is likely that the experimental transition energy of $S_2(\pi\pi^*)$ is slightly lower in energy with a value

around 4.5 eV. Inclusion of solvent effects in the B3LYP calculations leads to small hypsochromic shifts of 0.03 and 0.05 eV for the $S_1(n\pi^*)$ state of *trans-* and *cis-*azobenzene, respectively. These shifts are somewhat in disagreement with the measured values, which rather indicate small bathochromic shifts. Nevertheless, the larger bathochromic shift - comprised between -0.21 and -0.26 eV depending on the experimental data - observed for the $S_2(\pi\pi^*)$ state of *trans-*azobenzene is better reproduced by the calculations with a value of -0.16 eV. The calculated bathochromic shift of -0.13 eV for the $S_2(\pi\pi^*)$ state of *cis-*azobenzene is also in general agreement with the experimental values. The excitation energies obtained with PBE, which belongs to the generalized gradient approximation family of functionals, are in larger disagreement with experiment, giving values underestimated by more than 0.5 eV. However, the energies obtained with the hybrid functional M06-2X and the long-range corrected functionals CAM-B3LYP and ωB97X are in better agreement with the experimental results. In particular, the CAM-B3LYP functional provides the most accurate excitation energies. Indeed, when comparing to the experimental values of reference[46] recorded in ethanol solution, deviations of 0.01 and 0.05 eV are found for the $S_1(n\pi^*)$ and $S_2(\pi\pi^*)$ states of *trans-*azobenzene, respectively, and deviations of -0.04 and 0.35 eV are obtained for the $S_1(n\pi^*)$ and $S_2(\pi\pi^*)$ states of *cis-*azobenzene, respectively. The good performance of CAM-B3LYP for the $S_1(n\pi^*)$ and $S_2(\pi\pi^*)$ excitation energies is in agreement with a previous study.[73]

The excitation energies obtained with wave function based methods for the two states of interest are reported in Table 3. These calculations were performed in a vacuum employing the B3LYP geometry optimized in ethanol. The choice of the ground state geometry is motivated by the analysis of the vibrational frequencies and of the RR spectra (see section 3.3.). By comparing to the experimental results recorded in gas phase, the EOM-CCSD approach overestimates the excitation energies by 0.13 and 0.41 eV for the $S_1(n\pi^*)$ and $S_2(\pi\pi^*)$ states of *trans-*azobenzene, respectively, and by 0.08 eV and 0.09 eV for the $S_1(n\pi^*)$ and $S_2(\pi\pi^*)$ states of *cis-*azobenzene, respectively. These deviations are larger than those obtained with the best TDDFT functional i.e. CAM-B3LYP.

Next, as expected the SA-RASSCF excitation energies are much higher, with overestimations comprised between 0.5 and 2.0 eV. Moreover, it should be noticed that in the RASSCF(18,4,4;9,0,7) partition the dipole allowed $\pi\pi^*$ state is found as the S_6 and S_5 excited state for *trans*-azobenzene and *cis*-azobenzene, respectively. The inclusion of dynamical correlation leads to very accurate results. Indeed, the deviations with respect to the experimental values obtained with RASPT2(18,2,2;7,3,6) are only of -0.09 and 0.05 eV for the $S_1(n\pi^*)$ and $S_2(\pi\pi^*)$ states of *trans*-azobenzene, respectively, and of -0.09 eV and -0.11 eV for the $S_1(n\pi^*)$ and $S_2(\pi\pi^*)$ states of *cis*-azobenzene. Note that if an experimental value of about 4.5 eV is assumed for the $S_2(\pi\pi^*)$ state of *cis*-azobenzene (instead of 4.68 eV), the RASPT2(18,2,2;7,3,6) approach provides a more accurate result than EOM-CCSD for this state. Considering the results for the second partition RASPT2(18,4,4;9,0,7), it is seen that the energies for the $S_1(n\pi^*)$ states are nearly converged with respect to the active space size. Indeed, when going from the first to the second partition, variations of only 0.01 and -0.02 eV are obtained for *trans*-azobenzene and *cis*-azobenzene, respectively. However, larger variations are found for the $\pi\pi^*$ states. It is noteworthy that the $\pi\pi^*$ state of the RASSCF(18,4,4;9,0,7) reference wave function of *trans*-azobenzene is split into two states upon applying the MS-RASPT2 procedure at 4.30 (S_2) and 4.51 eV (S_4). The variation between both partitions is still moderate for *trans*-azobenzene (0.13 eV for S_2) but is much larger for *cis*-azobenzene (0.42 eV). This latter value can be related to the higher position of the $\pi\pi^*$ state, which is found as the S_5 state. Therefore, from the analysis of the excitation energies calculated with wave function based methods, it can be concluded that the most accurate results are obtained with the RASPT2(18,2,2;7,3,6) approach. Thus, an empty RAS2 subspace, as in RAS(18,4,4;9,0,7), is not beneficial in comparison to RAS(18,2,2;7,3,6), and this despite the increased excitation level from double to quadruple and despite the increased number of CSFs from merely 12601 to 274450.

Table 2: Excited state excitation energies (eV) obtained with TDDFT. In the notation TD-ESM//GSM, ESM and GSM indicate the methods employed for the excited and the ground states properties, respectively.

Methods	trans-azobenzene		cis-azobenzene	
	$S_1(n\pi^*)$	$S_2(\pi\pi^*)$	$S_1(n\pi^*)$	$S_2(\pi\pi^*)$
TD-B3LYP//B3LYP[a]	2.55	3.69	2.56	4.09
TD-B3LYP//B3LYP[b]	2.58	3.53	2.61	3.96
TD-PBE//PBE[b]	2.23	3.20	2.36	3.29
TD-M06-2X//M06-2X[b]	2.55	4.04	2.59	4.65
TD-CAM-B3LYP//CAM-B3LYP[b]	2.77	3.96	2.82	4.63
TD-ωB97X//ωB97X[b]	2.85	4.19	2.93	4.92
Exp. (gas phase)	2.82[c]	4.12[c]	2.92[c]	4.68[c]
Exp. (ethanol)	2.76[d]	3.91[d]	2.86[d]	4.28[d]
	2.95[e]	3.86[e]	2.8[e]	4.4[e]
	2.80[f]	3.89[f]	2.87[f]	4.42[f]

[a] Calculations performed in a vacuum. [b] Calculations performed in ethanol using PCM. [c] Experimental values in gas phase.[91,76] [d] Recorded in ethanol.[46] [e] Recorded in ethanol.[92,76] [f] Recorded in ethanol.[93,76]

Table 3: Excited state excitation energies (eV) obtained with EOM-CCSD, SA-RASSCF and MS-RASPT2. In the notation ESM//GSM, ESM and GSM indicate the methods employed for the excited and the ground states properties, respectively.

Methods[a]	trans-azobenzene		cis-azobenzene	
	$n\pi^*$	$\pi\pi^*$	$n\pi^*$	$\pi\pi^*$
EOM-CCSD//B3LYP	2.95 (S_1)	4.53 (S_2)	3.00 (S_1)	4.77 (S_2)
RASSCF(18,2,2;7,3,6)//B3LYP	3.37 (S_1)	5.85 (S_2)	3.68 (S_1)	5.90 (S_2)
RASSCF(18,4,4;9,0,7)//B3LYP	3.53 (S_1)	6.11 (S_6)	3.63 (S_1)	6.01 (S_5)
RASPT2(18,2,2;7,3,6)//B3LYP	2.73 (S_1)	4.17 (S_2)	2.83 (S_1)	4.57 (S_2)
RASPT2(18,4,4;9,0,7)//B3LYP	2.74 (S_1)	4.30 (S_2)	2.81 (S_1)	4.99 (S_5)
Exp. (gas phase)[b]	2.82	4.12	2.92	4.68

[a] The excited state calculations were performed in a vacuum using the B3LYP geometry optimized in ethanol. [b] Experimental values in gas phase.[91,76]

3.3. Comparison between (TD)DFT results and experimental RR data in ethanol.

The assessment of the excited states gradients is first performed by comparing the DFT and TDDFT results with respect to experimental RR spectra recorded in ethanol.[46] All calculations presented in this section made use of PCM for the computations of the geometries, frequencies and excited states gradients. The relative RR intensities were calculated using the STA formula (Eq. 1), which directly

relates the gradients to the RR intensities. A more sophisticated method[28,38] to compute RR intensities, which includes the vibronic structure described by the FC factors, was tested (Tables S10, S11) and showed only small differences with respect to the STA approach. Therefore, only results using the STA are presented here.

For *trans*-azobenzene, the gradients are assessed with respect to RR intensities recorded at an excitation wavelength of 406 nm i.e. excitation energy of 3.05 eV. This excitation energy lies in-between the energies of the dipole-forbidden $S_1(n\pi^*)$ state and dipole-allowed $S_2(\pi\pi^*)$ state. The investigation of the calculated vibrational signatures for each state revealed that the RR response at an excitation wavelength of 406 nm originates dominantly from the $S_2(\pi\pi^*)$ state. Therefore, the experimental data are compared to the computed RR intensities, i.e. gradients, of $S_2(\pi\pi^*)$. For *cis*-azobenzene, the gradients are assessed with respect to RR intensities recorded at an excitation wavelength of 458 nm i.e. excitation energy of 2.71 eV. This excitation energy is in resonance with the dipole-allowed $S_1(n\pi^*)$ state of *cis*-azobenzene. Therefore, in this case the experimental data are compared to the computed RR intensities of $S_1(n\pi^*)$.

The most RR active bands were assigned to the calculated vibrational modes (Figure 3 and Tables S12, S13). These modes correspond to totally symmetric vibrations, for which the excited state gradients are non-vanishing. The harmonic frequencies obtained with B3LYP, PBE, M06-2X, CAM-B3LYP, ωB97X and MP2 were corrected by the factors 0.98, 1.00, 0.95, 0.95, 0.95 and 0.98, respectively. The RMS deviations between the experimental and theoretical frequencies are given in Table 4. As it can be seen from Table 4, B3LYP provides the most accurate frequencies for the two isomers of azobenzene, whereas the other considered methods have significantly larger RMS deviations. The good performance of the B3LYP functional in reproducing the vibrational frequencies, IR and Raman intensities of azobenzene was already pointed out in a previous study[94] and was shown to be of comparable accuracy as MP2[95,76]. Therefore, the ground state geometry, frequencies and modes obtained with B3LYP were also employed to calculate excited state properties in association with different theoretical methods.

Table 4: RMS deviations between experimental[46] and calculated ground state vibrational frequencies of *trans*-azobenzene and *cis*-azobenzene.

Methods[a]	Frequency RMS deviations (cm^{-1})	
	trans-azobenzene	*cis*-azobenzene
B3LYP	10.1	14.9
PBE	22.2	26.5
M06-2X	35.8	28.9
CAM-B3LYP	29.1	24.3
ωB97X	37.0	22.6
MP2	25.2	17.3

[a] Frequencies calculated in ethanol using PCM.

For *trans*-azobenzene, the investigation of the RR intensity RMS deviations (Table 5) shows that B3LYP and PBE give accurate relative RR intensities with a RMS deviation of 0.34 (TD-B3LYP//B3LYP and TD-PBE//PBE). However, these two functionals present marked differences in the RR vibrational pattern. PBE is in better agreement with respect to experimental results for the three bands in the 1400-1500 cm^{-1} region (Figure 3). Indeed, it correctly reproduces the intensity of the most intense experimental band at 1440 cm^{-1}, whereas B3LYP shows different relative intensities for these three bands and its RR spectrum is dominated by the band at 1513 cm^{-1}. Nevertheless, PBE predicts less accurate RR intensities than B3LYP in the 1000-1200 cm^{-1} region and it underestimates the vibrational frequencies. The RR spectra obtained with M06-2X and with the long-range corrected functionals CAM-B3LYP and ωB97X show large disagreement with the measured spectrum, leading to RMS deviations on the RR intensities larger than 0.5. However, if these functionals are used for the excited states gradients in association with the B3LYP geometry, improved RR intensities are obtained with RMS deviations of 0.28 and 0.27. This behavior originates from a better reproduction of the 1400-1500 cm^{-1} region and indicates that these functionals provide good excited states gradients but show some inability to correctly describe the ground state normal coordinates of *trans*-azobenzene. The combination of PBE gradients with the B3LYP geometry (TD-PBE//B3LYP) gives a RR spectrum that is closer to the TD-B3LYP//B3LYP results than to the TD-PBE//PBE spectrum, particularly in the 1400-1500 cm^{-1} region. However, a

larger RMS deviation of 0.42 is obtained. These differences indicate that the choice of the method for the ground state normal coordinates has a strong impact on the resulting RR intensities, which is often larger than the effects of different methods on the excited states gradients.
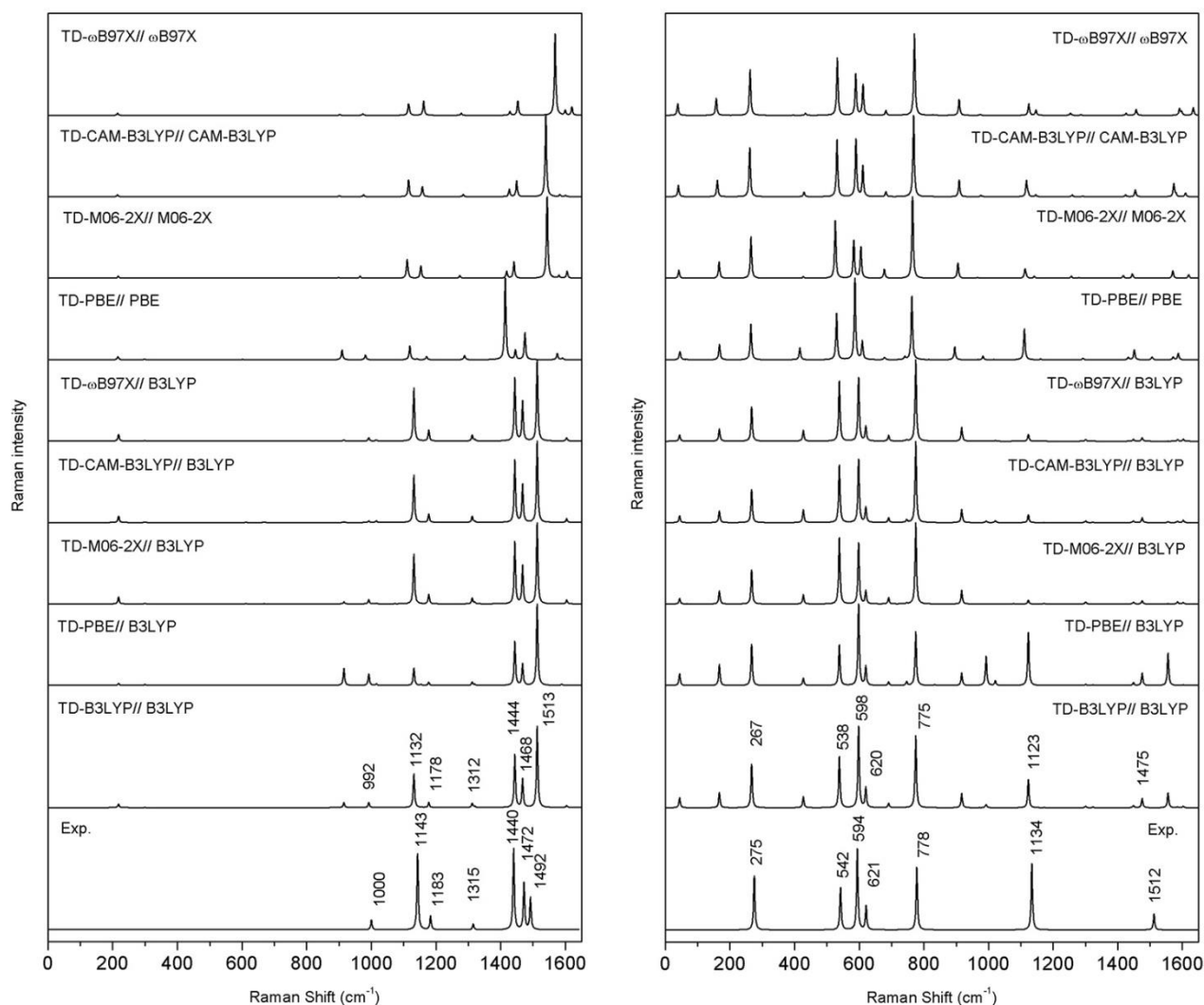

Figure 3: Comparison between calculated and experimental RR spectra of *trans*-azobenzene (left, $S_2(\pi\pi^*)$) and *cis*-azobenzene (right, $S_1(n\pi^*)$). In the notation TD-ESM//GSM, ESM and GSM indicate the methods employed for the excited and the ground states properties, respectively. The spectra are normalized with respect to the most intense band, and a Lorentzian function with a FWHM of 5 cm^{-1} is employed to broaden the transitions. The experimental RR spectra are reconstructed from the cross-sections reported in reference.[46]

For *cis*-azobenzene, the TD-B3LYP//B3LYP and TD-PBE//PBE methods give small RMS deviations with values of 0.20 and 0.19, respectively. Overall, these methods present also comparable vibrational patterns (Figure 3) that are in agreement with the experimental spectrum. Similarly to *trans*-azobenzene, the TD-M06-2X//M06-2X, TD-CAM-B3LYP//CAM-B3LYP and TD-ωB97X//ωB97X methods provide larger RMS deviations and present disagreements with the experimental spectrum in the 500-800 cm^{-1} region. Moreover, and contrary to *trans*-azobenzene, the association of these functionals with the B3LYP geometry does not improve the RMS deviations, which remain larger than 0.30. However, the TD-PBE//B3LYP method provides the best agreement with the measured spectrum, with a RMS deviation of only 0.10.

Table 5: RMS deviations between experimental and calculated relative RR intensities of *trans*-azobenzene and *cis*-azobenzene. In the notation TD-ESM//GSM, ESM and GSM indicate the methods employed for the excited and the ground states properties, respectively.

Methods[a]	RR intensity RMS deviations (arbitrary units)	
	trans-azobenzene[b]	*cis*-azobenzene[c]
TD-B3LYP//B3LYP	0.34 (0.35)	0.20 (0.22)
TD-PBE//B3LYP	0.42 (0.42)	0.10 (0.09)
TD-M06-2X//B3LYP	0.28 (0.29)	0.36 (0.36)
TD-CAM-B3LYP//B3LYP	0.28 (0.29)	0.32 (0.34)
TD-ωB97X//B3LYP	0.27 (0.28)	0.34 (0.34)
TD-PBE//PBE	0.34	0.19
TD-M06-2X//M06-2X	0.52	0.38
TD-CAM-B3LYP//CAM-B3LYP	0.52	0.29
TD-ωB97X//ωB97X	0.55	0.34

[a] Calculations performed in ethanol using PCM, values in brackets correspond to gradients calculated in a vacuum. [b] Experimental RR spectra[46] recorded at an excitation wavelength of 406 nm, the calculated ($S_2(\pi\pi^*)$) and measured RR intensities are normalized with respect to the band at 1440 cm^{-1}. [c] Experimental RR spectra[46] recorded at an excitation wavelength of 458 nm, the calculated ($S_1(n\pi^*)$) and measured RR intensities are normalized with respect to the band at 594 cm^{-1}.

In summary, the comparison between calculated and experimental RR spectra has shown that B3LYP provides the most accurate ground state vibrational frequencies. The RR spectra obtained

with TD-B3LYP//B3LYP and TD-PBE//PBE methods give a good agreement with the experimental spectra. The TD-M06-2X//B3LYP, TD-CAM-B3LYP//B3LYP and TD-ωB97X//B3LYP approaches improve the excited states gradients for the $S_2(\pi\pi^*)$ state of *trans*-azobenzene but not for the $S_1(n\pi^*)$ state of *cis*-azobenzene, which is better described by the TD-PBE//B3LYP method.

3.4. Comparison between wave function based methods and experimental RR spectra.

The RR spectra calculated with the EOM-CCSD, RASSCF and RASPT2 methods are compared to experimental results (Table 6 and Figure 4). The excited states gradients were calculated in a vacuum, whereas, according to the analysis of the previous section, the B3LYP properties obtained in ethanol are employed for the ground state. The EOM-CCSD gradients were computed with the 6-31G(d) basis set and the RASSCF as well as the RASPT2 gradients were obtained with the 6-311++G(d,p) basis set. The EOM-CCSD gradients of *trans*-azobenzene were also calculated with the 6-311+G(d) basis set to check the convergence of the results. Thus, almost equal RMS deviations of 0.28 and 0.27 are obtained with the 6-31G(d) and 6-311+G(d) basis sets, respectively (Table 6). Therefore, for *cis*-azobenzene the gradients were only computed with the 6-31G(d) basis set. Additionally, the TDDFT gradients were also re-calculated in a vacuum (Table 5 and Figure 4) to check the impact of the solvent on the RR spectra and to provide direct comparison with the wave function based methods. The results presented in Table 5 clearly indicate that the solvent has a small effect on the excited states gradients. Indeed, the RMS deviations are modified at the most by 0.02, which does not alter the conclusions obtained when comparing the different methods.

For *trans*-azobenzene, the comparison between the wave function based methods and the experimental RR spectrum shows that the RMS deviations obtained with the EOM-CCSD and RASSCF methods have comparable values to the best TDDFT approaches. In fact, the smallest RMS deviation is found with the RASSCF(18,2,2;7,3,6) method with a value of 0.24. The RMS deviations calculated with the RASPT2 methods are larger with a value of 0.38. This result is surprising because RASPT2 was expected to provide the most accurate gradients. For *cis*-

azobenzene, the RMS deviations computed with EOM-CCSD and RASSCF are larger than those obtained with the best TDDFT approaches. The RASPT2 results are in closer agreement to the experimental RR spectra providing a RMS deviation of 0.19 for the RASPT2(18,4,4;9,0,7) method. However, this value is still larger than the TD-PBE//B3LYP results of 0.09.

Table 6: RMS deviations between experimental and calculated relative RR intensities of *trans*-azobenzene and *cis*-azobenzene. In the notation TD-ESM//GSM, ESM and GSM indicate the methods employed for the excited and the ground states properties, respectively.

Methods[a]	RR intensity RMS deviations (arbitrary units)	
	trans-azobenzene[b]	*cis*-azobenzene[c]
EOM-CCSD//B3LYP[d]	0.28 (0.27)	0.27
RASSCF(18,2,2;7,3,6)//B3LYP	0.24	0.33
RASSCF(18,4,4;9,0,7)//B3LYP	0.30	0.37
RASPT2(18,2,2;7,3,6)//B3LYP	0.38	0.26
RASPT2(18,4,4;9,0,7)//B3LYP	0.38	0.19

[a] Gradients calculated in a vacuum using the B3LYP geometry in ethanol. [b] Experimental RR spectra[46] recorded at an excitation wavelength of 406 nm, the calculated ($\pi\pi^*$ state) and measured RR intensities are normalized with respect to the band at 1440 cm^{-1}. [c] Experimental RR spectra[46] recorded at an excitation wavelength of 458 nm, the calculated ($n\pi^*$ state) and measured RR intensities are normalized with respect to the band at 594 cm^{-1}. [d] The value in bracket is calculated with the 6-311+G(d) basis set.

The fact that the RMS deviations calculated with the RASPT2 method (using different RAS partitions) are larger than those obtained with RASSCF and EOM-CCSD (*trans*-azobenzene) or that they do not improve the TDDFT results, provides an indication that the comparison with experimental RR spectra is not fully adequate to assess the excited states gradients. The discrepancies with experiment might originate from several reasons: (i) inaccuracies in the B3LYP normal coordinates, (ii) solvent effects not described by PCM, (iii) limitations of the short-time approximation for RR intensities, (iv) effects arising from the large amplitudes in the zero-point vibrational movements[95], and finally (v) experimental errors. In particular, the analysis of section 3.3 has shown that the choice of the ground state normal coordinates has a significant impact on the

relative RR intensities. This is clearly visible in the case of *trans*-azobenzene in the 1400-1500 cm^{-1} region. Thus, it is likely that, despite the good vibrational frequencies obtained with B3LYP, some inaccuracies still remain for the normal modes. In order to investigate such effects further, the RR intensities were also calculated with B3LYP using the MP2 normal modes (TD-B3LYP//MP2). The obtained RR spectra (Figure S3) do not improve upon the TD-B3LYP//B3LYP results and lead to RMS deviations of 0.34 and 0.55 for *trans*-azobenzene and *cis*-azobenzene, respectively. Therefore, in order to separate the errors originating from the ground state properties and from the excited state properties, and to eliminate possible inaccuracies originating from the comparison with experimental data, the gradients are additionally assessed in the next section with respect to the RASPT2 results.
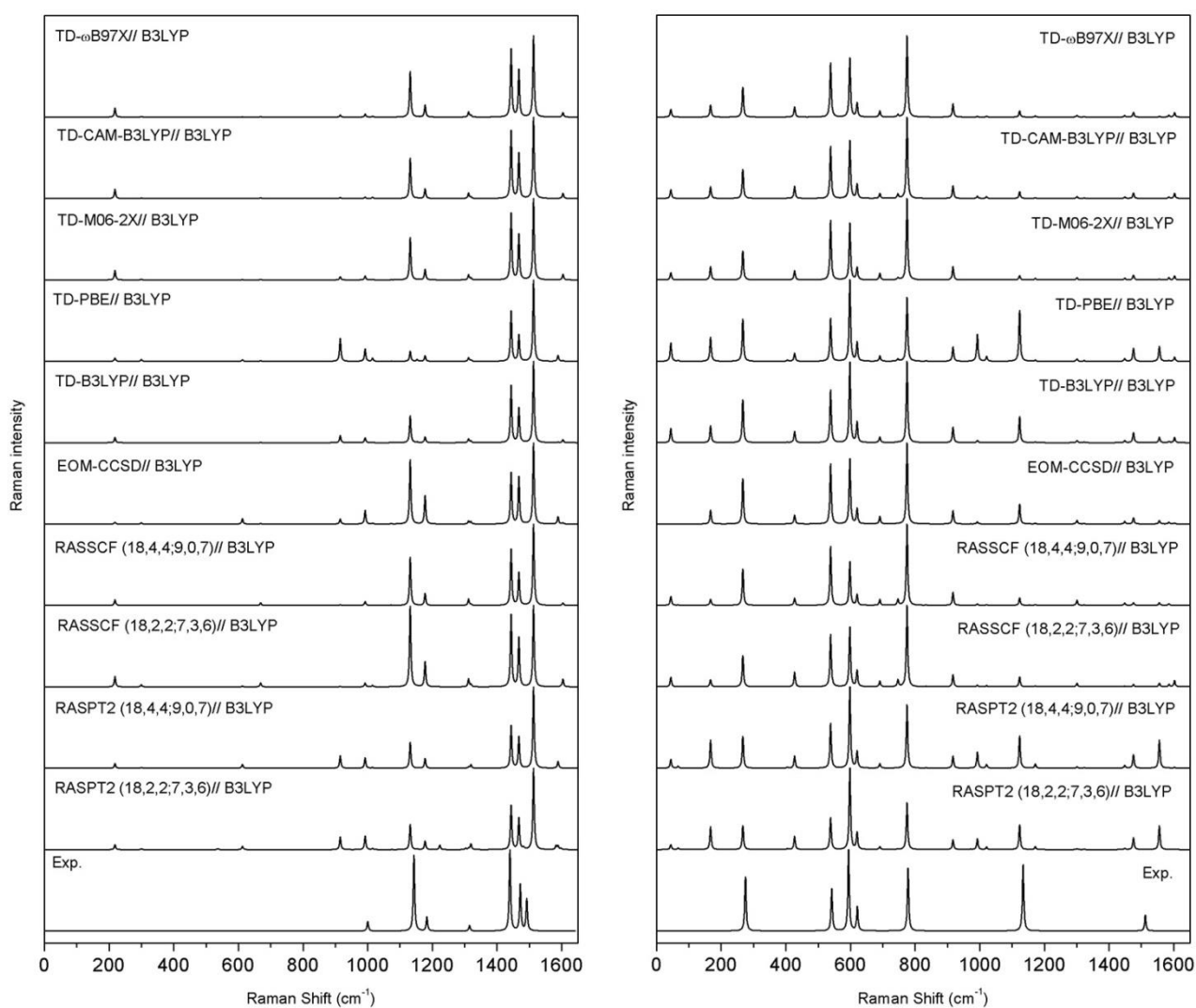
Figure 4: Comparison between calculated and experimental RR spectra of *trans*-azobenzene (left, ππ*) and *cis*-azobenzene (right, nπ*). In the notation TD-ESM//GSM, ESM and GSM indicate the methods employed for the excited and the ground states properties, respectively. The spectra are normalized with respect to the most intense band, and a Lorentzian function with a FWHM of 5 cm^{-1} is employed to broaden the transitions. The experimental RR spectra are reconstructed from the cross-sections reported in reference.[46]

3.5. Comparison of the different methods with respect to RASPT2(18,2,2;7,3,6).

In this section, the excited states gradients of both nπ* and ππ* states of *trans-* and *cis*-azobenzene are assessed with respect to the RASPT2(18,2,2;7,3,6) results. This method gives the most accurate excitation energies (section 3.2.) for the four considered states. Therefore, the gradients obtained at this level of theory are considered as a theoretical reference. Additionally, the convergence with respect to the choice of active space is investigated by virtue of the RASPT2(18,4,4;9,0,7) data. In the same way as in the previous section, all gradients are calculated in a vacuum using the B3LYP geometry obtained in ethanol. The geometry and modes calculated with B3LYP are chosen to facilitate the comparison with the results reported in the other sections of the paper.

The investigation of the RMS deviations (Table 7) for *trans*-azobenzene shows that the RASPT2(18,4,4;9,0,7) and RASPT2(18,2,2;7,3,6) methods provide nearly identical gradients. Indeed, the RMS deviations have values of 0.00 and 0.01 for the nπ* and ππ* states, respectively. This demonstrates that the results are converged with respect to the active space size and that the RASPT2(18,2,2;7,3,6) data can be considered as a reference to assess the other methods. Thus, it is seen that for both nπ* and ππ* states of *trans*-azobenzene, B3LYP provides the most accurate gradients and RR spectra (Figure 4 and Figure S4) with respect to the multiconfigurational reference data. Indeed, RMS deviations of 0.06 and 0.07 (Table 7) are obtained for the nπ* and ππ* states, respectively. The PBE functional gives good gradients for the ππ* state with a RMS deviation (0.08) comparable to B3LYP. However, larger errors are obtained with this functional for the nπ* state, which shows a RMS deviation of 0.17. M06-2X and the two long-range corrected functionals perform equally well for both states, leading to RMS deviations close to 0.15, which are nevertheless significantly larger than those obtained with B3LYP. The facts that PBE is less accurate for the nπ* state, and that M06-2X, CAM-B3LYP and ωB97X do not improve the gradients for the ππ* state, vary from the conclusions reported in section 3.3 when comparison was made with the experimental spectra. Among the wave function based approaches, EOM-CCSD provides very good gradients for the nπ* state (RMS deviation of 0.05), whereas it is less accurate

for the $\pi\pi^*$ state (RMS deviation of 0.18 with the larger basis set). The RASSCF(18,4,4;9,0,7) method provides smaller RMS deviations than RASSCF(18,2,2;7,3,6) with values of 0.09 and 0.13 for the $n\pi^*$ and $\pi\pi^*$ states, respectively.

Table 7: RMS deviations on the relative RR intensities for the different methods with respect to the reference method RASPT2(18,2,2;7,3,6). In the notation TD-ESM//GSM, ESM and GSM indicate the methods employed for the excited and the ground states properties, respectively.

Methods[a]	RR intensity RMS deviations (arbitrary units)			
	trans-azobenzene		cis-azobenzene	
	$n\pi^*$	$\pi\pi^*$	$n\pi^*$	$\pi\pi^*$
TD-B3LYP//B3LYP	0.06	0.07	0.21	0.09
TD-PBE//B3LYP	0.17	0.08	0.18	0.41
TD-M06-2X//B3LYP	0.14	0.15	0.26	0.15
TD-CAM-B3LYP//B3LYP	0.14	0.15	0.23	0.10
TD-ωB97X//B3LYP	0.14	0.17	0.24	0.09
EOM-CCSD//B3LYP[b]	0.05 (0.05)	0.23 (0.18)	0.25	0.35
RASSCF(18,2,2;7,3,6)//B3LYP	0.14	0.32	0.23	0.12
RASSCF(18,4,4;9,0,7)//B3LYP	0.09	0.13	0.29	0.13
RASPT2(18,4,4;9,0,7)//B3LYP	0.00	0.01	0.11	0.10

[a] Gradients calculated in a vacuum using the B3LYP geometry in ethanol. [b] The values in brackets are calculated with the 6-311+G(d) basis set.

For cis-azobenzene, the RASPT2(18,4,4;9,0,7) calculation leads to RMS deviations of 0.11 and 0.10 for the $n\pi^*$ and $\pi\pi^*$ states, respectively. This indicates that the gradients are not fully converged with respect to the active space size, which is correlated to the low weight of the $\pi\pi^*$ configuration of S_5 (see Table S9). Nevertheless, according to the calculated excitation energies (Table 3) and the high weights of the leading $n\pi^*$ and $\pi\pi^*$ configurations (Table S9), it is assumed that RASPT2(18,2,2;7,3,6) provides the reference results. For the $n\pi^*$ state, all considered methods give RMS deviations comprised between 0.18 and 0.29. The best gradients are obtained for the PBE and B3LYP functionals, with values of 0.18 and 0.21, respectively. For the $\pi\pi^*$ state, the B3LYP and the long-range corrected functionals (CAM-B3LYP and ωB97X) give the most accurate

gradients with RMS deviations close to 0.10. For this state, PBE and EOM-CCSD calculations lead to large errors.

4. Conclusions

The present study has provided a detailed theoretical analysis of the two isomers of azobenzene in the Franck-Condon region. The geometries, vibrational frequencies and normal coordinates were obtained by MP2 and by several DFT methods, namely B3LYP, PBE, M06-2X, CAM-B3LYP and ωB97X, and comparison with experimental data shows that the B3LYP functional gives the most accurate results for the ground state properties i.e. geometries and frequencies.

The excited state properties of the $S_1(n\pi^*)$ and $S_2(\pi\pi^*)$ states of *trans-* and *cis-*azobenzene were investigated by TDDFT, EOM-CCSD and by state-of-the-art RASPT2/RASSCF calculations. The analysis of the vertical excitation energies and their comparison with experimental values has revealed that the RASPT2(18,2,2;7,3,6) calculation provides the most accurate excitation energies with deviations of the order of 0.1 eV. Among the TDDFT methods, the CAM-B3LYP functional shows the best performance on the excitation energies. The excited state gradients were assessed through the calculation of RR intensities. The comparison with experimental RR spectra in resonance with the $S_2(\pi\pi^*)$ state of *trans-*azobenzene and with the $S_1(n\pi^*)$ state of *cis-*azobenzene indicated that the B3LYP and PBE functionals provide good gradients for both isomers. However, the large RMS deviations obtained for the RASPT2 calculations suggested that the comparison between theoretical and measured RR spectra suffers from some limitations, which might likely be attributed to inaccuracies in the calculated ground state normal coordinates. Therefore, the excited state gradients were also assessed with respect to the reference RASPT2(18,2,2;7,3,6) data. In that case, the most accurate gradients are obtained with B3LYP, whereas other functionals as well as the EOM-CCSD and RASSCF calculations give less consistent results.

In general, despite the tendency of B3LYP to underestimate the excitation energies, this functional provides the most balanced description of both ground and excited state properties for both isomers

of azobenzene in the FC region. Moreover, it can be mentioned that the computationally more demanding methods, RASSCF and EOM-CCSD, do not perform better for excited states gradients as the computationally cheap TDDFT method. This indicates that a larger amount of correlation effects should be included e.g. at the RASPT2 level, to outperform TDDFT. This conclusion holds in the FC region but is likely different if highly distorted geometries are considered, as those explored in excited state dynamics. In that case, multiconfigurational methods like RASSCF should perform better than TDDFT.
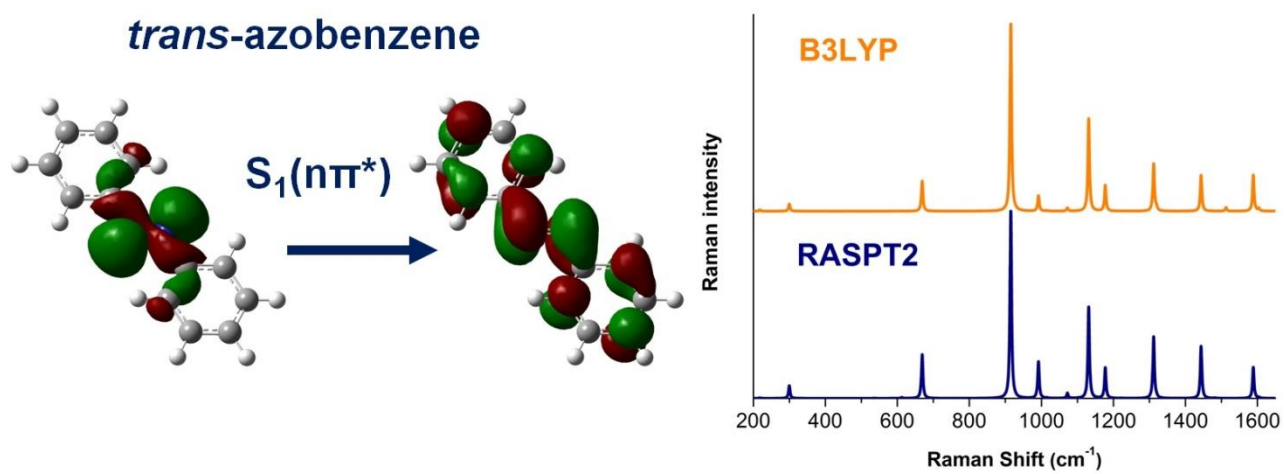
The good performance of TDDFT//DFT in reproducing experimental RR intensities within the STA was already reported by the some authors of this study on different molecules[28,96,29,97,30]. In particular, B3LYP was found accurate to describe the excitation energies and gradients of the first $\pi\pi^*$ state of rhodamine 6G[96] as well as of the metal-to-ligand charge transfer states of a ruthenium complex[97]. In the case of $\pi\pi^*$ transitions with a pronounced charge transfer character, long-range corrected functionals or hybrid functionals with a large amount of exact exchange were found more accurate for the excited state gradients, as for example in the case of the S_1 states of julolidinemalononitrile[28], of o-nitrophenol[29] and of a donor-acceptor thiazole-based chromophore[30]. For some of these systems[29,30], the wave function based methods CC2 and RASSCF provided gradients of comparable accuracy as TDDFT. Therefore, the results obtained herein for the azobenzene isomers confirm the good performance of TDDFT and also show that the assessment of the gradients should be preferably performed with respect to reference data calculated with highly correlated methods, like RASPT2, rather than with respect to experimental data.

Acknowledgments

Table of contents

trans-azobenzene

$S_1(n\pi^*)$

B3LYP

RASPT2

Raman intensity

Raman Shift (cm^{-1})

200 400 600 800 1000 1200 1400 1600

References

(1)   Biczysko, M.; Panek, P.; Scalmani, G.; Bloino, J.; Barone, V. Harmonic and Anharmonic Vibrational Frequency Calculations with the Double-Hybrid B2PLYP Method: Analytic Second Derivatives and Benchmark Studies. *J. Chem. Theory Comput.* **2010**, *6*, 2115–2125.

(2)   Puzzarini, C.; Biczysko, M.; Barone, V. Accurate Harmonic/anharmonic Vibrational Frequencies for Open-Shell Systems: Performances of the B3LYP/N07D Model for Semirigid Free Radicals Benchmarked by CCSD(T) Computations. *J. Chem. Theory Comput.* **2010**, *6*, 828–838.

(3)   Runge, E.; Gross, E. K. U. Density-Functional Theory for Time-Dependent Systems. *Phys. Rev. Lett.* **1984**, *52*, 997–1000.

(4)   Burke, K.; Werschnik, J.; Gross, E. K. U. Time-Dependent Density Functional Theory: Past, Present, and Future. *J. Chem. Phys.* **2005**, *123*, 62206.

(5)   Casida, M. E. Time-Dependent Density-Functional Theory for Molecules and Molecular Solids. *J. Mol. Struct. THEOCHEM* **2009**, *914*, 3–18.

(6)   Malmqvist, P. A.; Pierloot, K.; Shahi, A. R. M.; Cramer, C. J.; Gagliardi, L. The Restricted Active Space Followed by Second-Order Perturbation Theory Method: Theory and Application to the Study of CuO2 and Cu2O2 Systems. *J. Chem. Phys.* **2008**, *128*, 204109.

(7)   Malmqvist, P.-Å.; Rendell, A.; Roos, B. O. The Restricted Active Space Self-Consistent-Field Method, Implemented with a Split Graph Unitary Group Approach. *J. Phys. Chem.* **1990**, *94*, 5477–5482.

(8)   Olsen, J.; Roos, B. O.; Jørgensen, P.; Jensen, H. J. A. Determinant Based Configuration Interaction Algorithms for Complete and Restricted Configuration Interaction Spaces. *J. Chem. Phys.* **1988**, *89*, 2185.

(9)   Finley, J.; Malmqvist, P.-Å.; Roos, B. O.; Serrano-Andrés, L. The Multi-State CASPT2 Method. *Chem. Phys. Lett.* **1998**, *288*, 299–306.

(10) Roos, B. O. *Ab Initio Methods in Quantum Chemistry II*; Wiley-VCH: Chichester, U. K.,

1987.

(11)   Kállay, M.; Gauss, J. Calculation of Excited-State Properties Using General Coupled-Cluster and Configuration-Interaction Models. *J. Chem. Phys.* **2004**, *121*, 9257–9269.

(12)   Caricato, M.; Lipparini, F.; Scalmani, G.; Cappelli, C.; Barone, V. Vertical Electronic Excitations in Solution with the EOM-CCSD Method Combined with a Polarizable Explicit/Implicit Solvent Model. *J. Chem. Theory Comput.* **2013**, *9*, 3035–3042.

(13)   Stanton, J. F.; Bartlett, R. J. The Equation of Motion Coupled-Cluster Method. A Systematic Biorthogonal Approach to Molecular Excitation Energies, Transition Probabilities, and Excited State Properties. *J. Chem. Phys.* **1993**, *98*, 7029.

(14)   White, S. R. Density Matrix Formulation for Quantum Renormalization Groups. *Phys. Rev. Lett.* **1992**, *69*, 2863–2866.

(15)   White, S. R. Density-Matrix Algorithms for Quantum Renormalization Groups. *Phys. Rev. B* **1993**, *48*, 10345–10356.

(16)   Yanai, T.; Kurashige, Y.; Mizukami, W.; Chalupský, J.; Lan, T. N.; Saitow, M. Density Matrix Renormalization Group for Ab Initio Calculations and Associated Dynamic Correlation Methods: A Review of Theory and Applications. *Int. J. Quantum Chem.* **2015**, *115*, 283–299.

(17)   Stein, C. J.; Reiher, M. Automated Selection of Active Orbital Spaces. *J. Chem. Theory Comput.* **2016**, *12*, 1760–1771.

(18)   Laurent, A. D.; Jacquemin, D. TD-DFT Benchmarks: A Review. *Int. J. Quantum Chem.* **2013**, *113*, 2019–2039.

(19)   Sauri, V.; Serrano-andrés, L.; Shahi, A. R. M.; Gagliardi, L.; Vancoillie, S.; Pierloot, K. Multiconfigurational Second-Order Perturbation Theory Restricted Active Space (RASPT2) Method for Electronic Excited States: A Benchmark Study. *J. Chem. Theory Comput.* **2011**, *7*, 153–168.

(20)   González, L.; Escudero, D.; Serrano-Andrés, L. Progress and Challenges in the Calculation

of Electronic Excited States. *ChemPhysChem* **2012**, *13*, 28–51.

(21)   Schreiber, M.; Silva-Junior, M. R.; Sauer, S. P. A.; Thiel, W. Benchmarks for Electronically
Excited States: CASPT2, CC2, CCSD, and CC3. *J. Chem. Phys.* **2008**, *128*, 134110.

(22)   Miura, M.; Aoki, Y.; Champagne, B. Assessment of Time-Dependent Density Functional
Schemes for Computing the Oscillator Strengths of Benzene, Phenol, Aniline, and
Fluorobenzene. *J. Chem. Phys.* **2007**, *127*, 84103.

(23)   Dierksen, M.; Grimme, S. The Vibronic Structure of Electronic Absorption Spectra of Large
Molecules: A Time-Dependent Density Functional Study on the Influence of "Exact" Hartree
Fock Exchange. *J. Phys. Chem. A* **2004**, *108*, 10225–10237.

(24)   Santoro, F.; Lami, A.; Improta, R.; Bloino, J.; Barone, V. Effective Method for the
Computation of Optical Spectra of Large Molecules at Finite Temperature Including the
Duschinsky and Herzberg-Teller Effect: The Qx Band of Porphyrin as a Case Study. *J.
Chem. Phys.* **2008**, *128*, 224311.

(25)   Guthmuller, J.; Zutterman, F.; Champagne, B. Multimode Simulation of Dimer Absorption
Spectra from First Principles Calculations: Application to the 3,4,9,10-
Perylenetetracarboxylic Diimide Dimer. *J. Chem. Phys.* **2009**, *131*, 154302.

(26)   Karasulu, B.; Götze, J. P.; Thiel, W. Assessment of Franck-Condon Methods for Computing
Vibrationally Broadened UV-Vis Absorption Spectra of Flavin Derivatives: Riboflavin,
Roseoflavin, and 5-Thioflavin. *J. Chem. Theory Comput.* **2014**, *10*, 5549–5566.

(27)   Hodecker, M.; Biczysko, M.; Dreuw, A.; Barone, V. Simulation of Vacuum UV Absorption
and Electronic Circular Dichroism Spectra of Methyl Oxirane: The Role of Vibrational
Effects. *J. Chem. Theory Comput.* **2016**, *12*, 2820–2833.

(28)   Guthmuller, J.; Champagne, B. Time Dependent Density Functional Theory Investigation of
the Resonance Raman Properties of the Julolidinemalononitrile Push-Pull Chromophore in
Various Solvents. *J. Chem. Phys.* **2007**, *127*, 164507.

(29)   Guthmuller, J. Assessment of TD-DFT and CC2 Methods for the Calculation of Resonance

Raman Intensities: Application to O-Nitrophenol. *J. Chem. Theory Comput.* **2011**, *7*, 1082–1089.

(30) Kupfer, S.; Guthmuller, J.; González, L. An Assessment of RASSCF and TDDFT Energies and Gradients on an Organic Donor–Acceptor Dye Assisted by Resonance Raman Spectroscopy. *J. Chem. Theory Comput.* **2013**, *9*, 543–554.

(31) Petrenko, T.; Neese, F. Efficient and Automatic Calculation of Optical Band Shapes and Resonance Raman Spectra for Larger Molecules within the Independent Mode Displaced Harmonic Oscillator Model. *J. Chem. Phys.* **2012**, *137*, 234107.

(32) Silverstein, D. W.; Govind, N.; Dam, H. J. J. Van; Jensen, L. Simulating One-Photon Absorption and Resonance Raman Scattering Spectra Using Analytical Excited State Energy Gradients within Time-Dependent Density Functional Theory. *J. Chem. Theory Comput.* **2013**, *9*, 5490–5503.

(33) Ma, H.; Liu, J.; Liang, W. Time-Dependent Approach to Resonance Raman Spectra Including Duschinsky Rotation and Herzberg-Teller Effects: Formalism and Its Realistic Applications. *J. Chem. Theory Comput.* **2012**, *8*, 4474–4482.

(34) Egidi, F.; Bloino, J.; Cappelli, C.; Barone, V. A Robust and Effective Time-Independent Route to the Calculation of Resonance Raman Spectra of Large Molecules in Condensed Phases with the Inclusion of Duschinsky, Herzberg−Teller, Anharmonic, and Environmental Effects. *J. Chem. Theory Comput.* **2014**, *10*, 346–363.

(35) Neugebauer, J.; Hess, B. A. Resonance Raman Spectra of Uracil Based on Kramers-Kronig Relations Using Time-Dependent Density Functional Calculations and Multireference Perturbation Theory. *J. Chem. Phys.* **2004**, *120*, 11564–77.

(36) Romanova, J.; Liégeois, V.; Champagne, B. Resonant Raman Spectra of Molecules with Diradical Character: Multiconfigurational Wavefunction Investigation of Neutral Viologens. *Phys. Chem. Chem. Phys.* **2014**, *16*, 21721–21731.

(37) Wächtler, M.; Guthmuller, J.; González, L.; Dietzek, B. Analysis and Characterization of

Coordination Compounds by Resonance Raman Spectroscopy. *Coord. Chem. Rev.* **2012**, *256*, 1479–1508.

(38)   Guthmuller, J. Comparison of Simplified Sum-over-State Expressions to Calculate Resonance Raman Intensities Including Franck-Condon and Herzberg-Teller Effects. *J. Chem. Phys.* **2016**, *144*, 64106.

(39)   Heller, E. J.; Sundberg, R. L.; Tannor, D. Simple Aspects of Raman Scattering. *J. Phys. Chem.* **1982**, *86*, 1822–1833.

(40)   Bandara, H. M. D.; Burdette, S. C. Photoisomerization in Different Classes of Azobenzene. *Chem. Soc. Rev.* **2012**, *41*, 1809–1825.

(41)   Beharry, A. A.; Woolley, G. A. Azobenzene Photoswitches for Biomolecules. *Chem. Soc. Rev.* **2011**, *40*, 4422–4437.

(42)   Tan, E. M. M.; Amirjalayer, S.; Smolarek, S.; Vdovin, A.; Zerbetto, F.; Buma, W. J. Fast Photodynamics of Azobenzene Probed by Scanning Excited-State Potential Energy Surfaces Using Slow Spectroscopy. *Nat. Commun.* **2015**, *6*, 5860.

(43)   Dobryakov, A. L.; Quick, M.; Ioffe, I. N.; Granovsky, A. A.; Ernsting, N. P.; Kovalenko, S. A. Excited-State Raman Spectroscopy with and without Actinic Excitation: S1 Raman Spectra of Trans-Azobenzene. *J. Chem. Phys.* **2014**, *140*, 184310.

(44)   Quick, M.; Dobryakov, A. L.; Gerecke, M.; Richter, C.; Berndt, F.; Ioffe, I. N.; Granovsky, A. A.; Mahrwald, R.; Ernsting, N. P.; Kovalenko, S. A. Photoisomerization Dynamics and Pathways of Trans- and Cis-Azobenzene in Solution from Broadband Femtosecond Spectroscopies and Calculations. *J. Phys. Chem. B* **2014**, *118*, 8756–8771.

(45)   Chowdary, P. D.; Umapathy, S. Ultrafast Dynamics and Photochemistry of Pi-Pi* Excited Trans-Azobenzene - a Comprehensive Analysis of Resonance Raman Intensities. *J. Raman Spectrosc.* **2008**, *39*, 1538–1555.

(46)   Stuart, C. M.; Frontiera, R. R.; Mathies, R. A. Excited-State Structure and Dynamics of Cis- and Trans-Azobenzene from Resonance Raman Intensity Analysis. *J. Phys. Chem. A* **2007**,

111, 12072–12080.

(47) Chang, C. W.; Lu, Y. C.; Wang, T. Te; Diau, E. W. G. Photoisomerization Dynamics of Azobenzene in Solution with S1 Excitation: A Femtosecond Fluorescence Anisotropy Study. *J. Am. Chem. Soc.* **2004**, *126*, 10109–10118.

(48) Satzger, H.; Root, C.; Braun, M. Excited-State Dynamics of Trans- and Cis-Azobenzene after UV Excitation in the Pipi* Band. *J. Phys. Chem. A* **2004**, *108*, 6265–6271.

(49) Fujino, T.; Tahara, T. Picosecond Time-Resolved Raman Study of Trans-Azobenzene. *J. Phys. Chem. A* **2000**, *104*, 4203–4210.

(50) Lednev, I. K.; Ye, T.-Q.; Matousek, P.; Towrie, M.; Foggi, P.; Neuwahl, F. V. R.; Umapathy, S.; Hester, R. E.; Moore, J. N. Femtosecond Time-Resolved UV-Visible Absorption Spectroscopy of Trans-Azobenzene: Dependence on Excitation Wavelength. *Chem. Phys. Lett.* **1998**, *290*, 68–74.

(51) Nägele, T.; Hoche, R.; Zinth, W.; Wachtveitl, J. Femtosecond Photoisomerization of Cis-Azobenzene. *Chem. Phys. Lett.* **1997**, *272*, 489–495.

(52) Gámez, J. a; Weingart, O.; Koslowski, A.; Thiel, W. Periodic Decay in the Photoisomerisation of P-Aminoazobenzene. *Phys. Chem. Chem. Phys.* **2013**, *15*, 11814–11821.

(53) Harabuchi, Y.; Ishii, M.; Nakayama, A.; Noro, T.; Taketsugu, T. A Multireference Perturbation Study of the NN Stretching Frequency of Trans-Azobenzene in Nπ∗ Excitation and an Implication for the Photoisomerization Mechanism. *J. Chem. Phys.* **2013**, *138*, 64305.

(54) Cusati, T.; Granucci, G.; Persico, M. Photodynamics and Time-Resolved Fluorescence of Azobenzene in Solution: A Mixed Quantum-Classical Simulation. *J. Am. Chem. Soc.* **2011**, *133*, 5109–5123.

(55) Böckmann, M.; Doltsinis, N. L.; Marx, D. Nonadiabatic Hybrid Quantum and Molecular Mechanic Simulations of Azobenzene Photoswitching in Bulk Liquid Environment. *J. Phys. Chem. A* **2010**, *114*, 745–754.

(56) Tiberio, G.; Muccioli, L.; Berardi, R.; Zannoni, C. How Does the Trans-Cis Photoisomerization of Azobenzene Take Place in Organic Solvents? *ChemPhysChem* **2010**, *11*, 1018–1028.

(57) Wang, L.; Xu, W.; Yi, C.; Wang, X. Isomerization and Electronic Relaxation of Azobenzene after Being Excited to Higher Electronic States. *J. Mol. Graph. Model.* **2009**, *27*, 792–796.

(58) Conti, I.; Garavelli, M.; Orlandi, G. The Different Photoisomerization Efficiency of Azobenzene in the Lowest Npi* and Pipi* Singlets: The Role of a Phantom State. *J. Am. Chem. Soc.* **2008**, *130*, 5216–5230.

(59) Yuan, S.; Dou, Y.; Wu, W.; Hu, Y.; Zhao, J. Why Does Trans-Azobenzene Have a Smaller Isomerization Yield for $\Pi\pi^*$ Excitation than for $N\pi^*$ Excitation? *J. Phys. Chem. A* **2008**, *112*, 13326–13334.

(60) Crecca, C. R.; Roitberg, A. E. Theoretical Study of the Isomerization Mechanism of Azobenzene and Disubstituted Azobenzene Derivatives. *J. Phys. Chem. A* **2006**, *110*, 8188–8203.

(61) Tiago, M. L.; Ismail-Beigi, S.; Louie, S. G. Photoisomerization of Azobenzene from First-Principles Constrained Density-Functional Calculations. *J. Chem. Phys.* **2005**, *122*, 94311.

(62) Toniolo, A.; Ciminelli, C.; Persico, M.; Martínez, T. J. Simulation of the Photodynamics of Azobenzene on Its First Excited State: Comparison of Full Multiple Spawning and Surface Hopping Treatments. *J. Chem. Phys.* **2005**, *123*, 234308.

(63) Cembran, A.; Bernardi, F.; Garavelli, M.; Gagliardi, L.; Orlandi, G. On the Mechanism of the Cis-Trans Isomerization in the Lowest Electronic States of Azobenzene: S0, S1, and T1. *J. Am. Chem. Soc.* **2004**, *126*, 3234–3243.

(64) Diau, E. W. A New Trans-to-Cis Photoisomerization Mechanism of Azobenzene on the S1(n,π*) Surface. *J. Phys. Chem. A* **2004**, *108*, 950–956.

(65) Ishikawa, T.; Noro, T.; Shoda, T. Theoretical Study on the Photoisomerization of Azobenzene. *J. Chem. Phys.* **2001**, *115*, 7503.

(66) Fan, G.; Liu, J.; He, G. Nonadiabatic Dynamics Study of Bridged-Azobenzene by the Time-Dependent Density Functional Tight-Binding Method. *Comput. Theor. Chem.* **2013**, *1023*, 10–18.

(67) Böckmann, M.; Doltsinis, N. L.; Marx, D. Enhanced Photoswitching of Bridged Azobenzene Studied by Nonadiabatic Ab Initio Simulation. *J. Chem. Phys.* **2012**, *137*, 22A505.

(68) Floß, G.; Granucci, G.; Saalfrank, P. Surface Hopping Dynamics of Direct Trans → Cis Photoswitching of an Azobenzene Derivative in Constrained Adsorbate Geometries. *J. Chem. Phys.* **2012**, *137*, 234701.

(69) Adamo, C.; Barone, V. Toward Reliable Density Functional Methods without Adjustable Parameters: The PBE0 Model. *J. Chem. Phys.* **1999**, *110*, 6158–6170.

(70) Lee, C.; Yang, W.; Parr, R. G. Development of the Colle-Salvetti Correlation-Energy Formula into a Functional of the Electron Density. *Phys. Rev. B* **1988**, *37*, 785–789.

(71) Becke, A. D. Density-Functional Thermochemistry. III. The Role of Exact Exchange. *J. Chem. Phys.* **1993**, *98*, 5648–5652.

(72) Yanai, T.; Tew, D. P.; Handy, N. C. A New Hybrid Exchange-Correlation Functional Using the Coulomb-Attenuating Method (CAM-B3LYP). *Chem. Phys. Lett.* **2004**, *393*, 51–57.

(73) Jacquemin, D.; Perpète, E. A.; Scuseria, G. E.; Ciofini, I.; Adamo, C. Extensive TD-DFT Investigation of the First Electronic Transition in Substituted Azobenzenes. *Chem. Phys. Lett.* **2008**, *465*, 226–229.

(74) Escudero, D.; Trupp, S.; Bussemer, B.; Mohr, G. J.; González, L. Spectroscopic Properties of Azobenzene-Based pH Indicator Dyes: A Quantum Chemical and Experimental Study. *J. Chem. Theory Comput.* **2011**, *7*, 1062–1072.

(75) Gagliardi, L.; Orlandi, G.; Bernardi, F.; Cembran, A.; Garavelli, M. A Theoretical Study of the Lowest Electronic States of Azobenzene: The Role of Torsion Coordinate in the Cis–trans Photoisomerization. *Theor. Chem. Acc.* **2004**, *111*, 363–372.

(76) Fliegl, H.; Köhn, A.; Hättig, C.; Ahlrichs, R. Ab Initio Calculation of the Vibrational and

Electronic Spectra of Trans- and Cis-Azobenzene. *J. Am. Chem. Soc.* **2003**, *125*, 9821–9827.

(77) Hoffman, D. P.; Ellis, S. R.; Mathies, R. A. Low Frequency Resonant Impulsive Raman Modes Reveal Inversion Mechanism for Azobenzene. *J. Phys. Chem. A* **2013**, *117*, 11472– 11478.

(78) Perdew, J. P.; Burke, K.; Ernzerhof, M. Generalized Gradient Approximation Made Simple. *Phys. Rev. Lett.* **1996**, *77*, 3865–3868.

(79) Zhao, Y.; Truhlar, D. G. The M06 Suite of Density Functionals for Main Group Thermochemistry, Thermochemical Kinetics, Noncovalent Interactions, Excited States, and Transition Elements: Two New Functionals and Systematic Testing of Four M06-Class Functionals and 12 Other Function. *Theor. Chem. Acc.* **2008**, *120*, 215–241.

(80) Chai, J. Da; Head-Gordon, M. Systematic Optimization of Long-Range Corrected Hybrid Density Functionals. *J. Chem. Phys.* **2008**, *128*.

(81) Merrick, J. P.; Moran, D.; Radom, L. An Evaluation of Harmonic Vibrational Frequency Scale Factors. *J. Phys. Chem. A* **2007**, *111*, 11683–11700.

(82) Tomasi, J.; Mennucci, B.; Cammi, R. Quantum Mechanical Continuum Solvation Models. *Chem. Rev.* **2005**, *105*, 2999–3093.

(83) Frisch, M. J.; Trucks, G. W.; Schlegel, H. B.; Scuseria, G. E.; Robb, M. A.; Cheeseman, J. R.; Scalmani, G.; Barone, V.; Mennucci, B.; Petersson, G. A.; et al. *Gaussian 09, Revision A.02*; Gaussian, Inc., Wallingford CT, 2009.

(84) Aquilante, F.; Autschbach, J.; Carlson, R. K.; Chibotaru, L. F.; Delcey, M. G.; De Vico, L.; Fdez. Galván, I.; Ferré, N.; Frutos, L. M.; Gagliardi, L.; et al. Molcas 8: New Capabilities for Multiconfigurational Quantum Chemical Calculations across the Periodic Table. *J. Comput. Chem.* **2016**, *37*, 506–541.

(85) Aquilante, F.; Malmqvist, P. Å.; Pedersen, T. B.; Ghosh, A.; Roos, B. O. Cholesky Decomposition-Based Multiconfiguration Second-Order Perturbation Theory (CD-CASPT2): Application to the Spin-State Energetics of CoIII(diiminato)(NPh). *J. Chem. Theory Comput.*

2008, *4*, 694–702.

(86)   Malmqvist, P.-Å.; Roos, B. O. The CASSCF State Interaction Method. *Chem. Phys. Lett.* **1989**, *155*, 189–194.

(87)   Biswas, N.; Umapathy, S. Density Functional Calculations of Structures, Vibrational Frequencies, and Normal Modes of Trans- and Cis-Azobenzene. *J. Phys. Chem. A* **1997**, *101*, 5555–5566.

(88)   Bouwstra, J. a.; Schouten, A.; Kroon, J. Structural Studies of the System Trans-Azobenzene/trans-Stilbene. I. A Reinvestigation of the Disorder in the Crystal Structure of Trans-Azobenzene, C12H10N2. *Acta Crystallogr. Sect. C Cryst. Struct. Commun.* **1983**, *39*, 1121–1123.

(89)   Mostad, A.; Rømming, C. A Refinement of the Crystal Structure of Cis-Azobenzene. *Acta Chemica Scandinavica*, 1971, *25*, 3561–3568.

(90)   Traetteberg, M.; Hillmo, I.; Hagen, K. A Gas Electron Diffraction Study of the Molecular Structure of Trans-Azobenzene. *J. Mol. Struct.* **1977**, *39*, 231–239.

(91)   Andersson, J.-Å.; Petterson, R.; Tegnér, L. Flash Photolysis Experiments in the Vapour Phase at Elevated Temperatures I: Spectra of Azobenzene and the Kinetics of Its Thermal Cis-Trans Isomerization. *J. Photochem.* **1982**, *20*, 17–32.

(92)   Jaffé, H. H.; Yeh, S.-J.; Gardner, R. W. The Electronic Spectra of Azobenzene Derivatives and Their Conjugate Acids. *J. Mol. Spectrosc.* **1958**, *2*, 120–136.

(93)   Birnbaum, P. P.; Linford, J. H.; Style, D. W. G. The Absorption Spectra of Azobenzene and Some Derivatives. *Trans. Faraday Soc.* **1953**, *49*, 735–744.

(94)   Stepanić, V.; Baranović, G.; Smrečki, V. Structure and Vibrational Spectra of Conjugated Acids of Trans- and Cis-Azobenzene. *J. Mol. Struct.* **2001**, *569*, 89–109.

(95)   Duarte, L.; Fausto, R.; Reva, I. Structural and Spectroscopic Characterization of E- and Z-Isomers of Azobenzene. *Phys. Chem. Chem. Phys.* **2014**, *16*, 16919–16930.

(96)   Guthmuller, J.; Champagne, B. Resonance Raman Scattering of Rhodamine 6G as Calculated

by Time-Dependent Density Functional Theory: Vibronic and Solvent Effects. *J. Phys. Chem. A* **2008**, *112*, 3215–3223.

(97)　Kupfer, S.; Guthmuller, J.; Wächtler, M.; Losse, S.; Rau, S.; Dietzek, B.; Popp, J.; González, L. Protonation Effects on the Resonance Raman Properties of a Novel (terpyridine)Ru(4H-Imidazole) Complex: An Experimental and Theoretical Case Study. *Phys. Chem. Chem. Phys.* **2011**, *13*, 15580–15588.